Mixed Longitudinal - Lateral Stability Control of Electric Vehicle Based on Online Tire - Road Friction Coefficients Estimation

Saeed Rezapour, Mohammad Ali Hamed [iD] *, Jafar Keighobadi

Department of Mechanical engineering, University of Tabriz, Tabriz, Iran

ABSTRACT: In this paper, a two-layer stability control system based on output feedback is designed for electric vehicles with four in-wheel motors using super twisting sliding mode control and extended Kalman filter. The joint-extended Kalman filter method is used at the same time for estimating the state of the vehicle and the friction coefficients between the wheels and the road. In the upper layer controller, the control torque required to ensure the lateral stability of the vehicle is calculated. In the second layer, by using torque vectoring, the required traction forces for each wheel are determined so that the control torque calculated in the first layer is provided. Then the corresponding slip rates are calculated for the new adjusted longitudinal forces. Using the obtained slip rates as the desired slip rate for each wheel, the required wheel torques are computed by using appropriate longitudinal controller. Using the Kalman filter largely eliminates the effects of sensor noise and structural uncertainty on estimated parameters. The present algorithm can calculate the control inputs for the lateral and longitudinal control of the vehicle, as well as estimate the state of the system and estimate the friction coefficients between the wheels and the road at the same time. The results show the efficiency of the designed control system which is discussed on different maneuvers.

1- Introduction

In recent years, a series of ecological problems and limitations due to the lack of fossil fuels led to more researches have been considered on the replacement of electric vehicles (EVs) with conventional vehicles powered by an internal combustion engine. Among the types of designs used for EVs , those driven by four in-wheel-motors (IWMs) inside each tire, have been considered as popular architecture for their advantages compared with other kinds of EVs [1].

In this kind of EVs; the removal of the transmission mechanism can improve the energy efficiency, and the total weight of the vehicle can be reduced, which is directly related to production cost. However, in EVs with IWMs due to the independent action of each wheel, the controllability of the system increases which ensures a more flexible response in different situations. Therefore, it seems that the use of this model is more suitable for EVs than other more complex models[2].

Today, many advanced cars are compared with each other in terms of their ability to provide safety and comfort to the passengers. To this end, the use of vehicle stability control systems has been given a lot of attention. The most determining aspects of stability in these vehicles, due to their weight range and the center of gravity height, are longitudinal and lateral stability systems [3, 4].

In these systems, the primary objective is to precisely follow the reference path by minimizing tracking errors. Typically, achieving effective path-following requires accounting for both longitudinal and lateral control during the tracking process [5]. For a simultaneous longitudinal–lateral control strategy, an appropriate tracking algorithm should be used. Modern control methods in EVs with four IWMs, generally use one lateral controller for direct yaw moment control and four longitudinal controllers in each IWM using different tracking algorithms. Some of these methods are:

Pure tracking control: The structure and concept of pure tracking control are straightforward and cost-effective. However, it is effective primarily for achieving optimal tracking results on roads with low to medium speeds and high friction coefficients [6].

PID: PID control offers the benefits of a simple structure, straightforward parameter adjustment, and robustness. Nevertheless, it is best suited for single-input-single-output linear time-varying systems rather than multi-input-multi-output time-varying DYC systems [7].

LQR: This approach requires developing an objective function using a precise model, with the control effectiveness strongly linked to the model's accuracy. Clearly, employing a controller with weak robustness of this kind is unsuitable for uncertain conditions in the problem being studied [8]. Some references have also used this approach in the design of an electric vehicle with IWMs[9].

*Corresponding author's email: ma.hamed@tabrizu.ac.ir

MPC: The model predictive control (MPC) approach has been utilized for EVs with IWMs. However, its limitations include the high computational demand of iterative matrix calculations and the complexity of managing multiple variables [10-12].

Fuzzy Control: Although a fuzzy controller has the advantage of solving nonlinear problems, its control rules are complex and the membership function is obtained according to mature experience, so it cannot be the best choice for vehicle stability [13].

SMC: In recent years, the sliding mode control method and its different types have been widely used as a tracking algorithm and it has appropriate results by considering the conditions of the problem [14]. Using this method by combining it with other methods including, neural network[15, 16], nonlinear disturbance observer[17], fuzzy controller[18, 19], and some other methods has led to the creation of different algorithms for various applications using it.

In this work, five super twisting SMC algorithms are used for lateral and longitudinal stability control of EV, in the hierarchical two-layer format [20]. In the upper layer, one SMC algorithm is designed for DYC and calculation of the control yaw moment. In the lower layer, four SMCs are used for each wheel's longitudinal stability considering the torque vectoring strategy which is required for applying the control yaw moment calculated in the upper layer[21].

Due to the complex and variable driving conditions, accurate road and vehicle parameters should be known or estimated. In this regard, the tire-road friction coefficient (TRFC), is one of the most important parameters has to be estimated. The two main methods are cause-based and effect-based methods [22]. Cause-based methods are performed using some expensive, sensitive, and unusual acoustic and optical sensors, which are unreasonable and difficult to use for commercial vehicles in the market. Therefore, the use of effect-based methods are considered in TRFC estimation. In this approach, TRFC is identified based on the vehicle dynamic response on varying road conditions [23].

By applying various types of observers or filters on the data obtained from the sensors, the effect of noise and uncertainties in these data can be minimized and the real states of the car can be estimated. In this paper, the Extended Kalman filter (EKF) is used for state estimation. As mentioned, various papers and references have been published both in the field of stability control of electric vehicles and in the field of using different filters. What has received less attention is the estimation of the states and TRFC online and simultaneously with the work of the stability controller and the use of direct feedback of friction coefficients in the calculation of control inputs. By applying some changes in the filter equations, using joint-EKF, the method can be used to estimate simultaneously TRFCs and vehicle state. Since the method is effect-based and TRFCs are estimated online. By applying these accurate and modified parameters to the equations and controllers of the upper and lower layers, the modeling becomes more accurate, and maintaining the stability of the vehicle despite

measurable uncertainties and noises can be achieved.

In the following section, mathematical and dynamic models are described. In this section, the 7-degree-of-freedom vehicle model, controller structure, and filter type are discussed. In section 3, the simulation results are presented and the efficiency of the proposed method in different situations is discussed. Finally, conclusions are given in section 4.

2- Modeling and Formulation

In this section, the vehicle dynamic model, controller structure, and joint filter structure are discussed. For the vehicle model, a 7-degree of freedom model has been employed, which is presented in sections 2-1. Then, the two-layer controller structure and its algorithm are presented in section 2-2, and subsequently, in section 2-3, explanations related to the joint-EKF filter-estimator structure are provided.

2- 1- Seven degree of freedom (7DOF) vehicle model

For the dynamic model of the car, the following assumptions are considered. The road is considered to be flat, without longitudinal or lateral slope, the roll and pitch dynamics have been ignored, and the vertical movement with the suspension system of the car is not taken into account.

To model the vehicle dynamics, a four-wheel car model with three degrees of freedom in the x-y plane, Fig.1, is considered [24]. According to this, the dynamic equations of motion are expressed as follows [25] .

$$m\dot{V_x} = \left(F_{xfl} + F_{xfr}\right)\cos\delta - \left(F_{yfl} + F_{yfr}\right)\sin\delta + F_{xrl} + F_{xrr} - F_{loss} + mV_y r \quad (1)$$

$$m\dot{V_y} = \left(F_{yfl} + F_{yfr}\right)\cos\delta + \left(F_{xfl} + F_{xfr}\right)\sin\delta + F_{yrl} + F_{yrr} - mV_x r \quad (2)$$
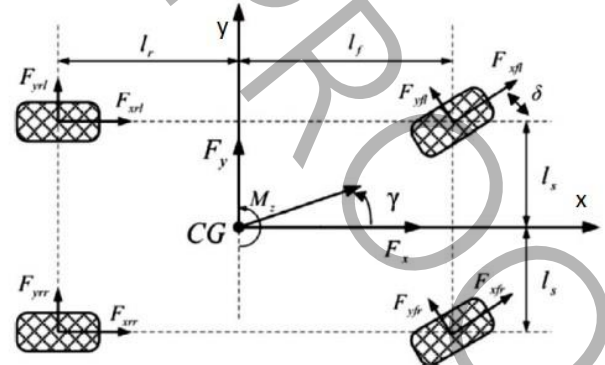
Fig. 1. Four-wheel vehicle model [22]

$$I_z \dot{r} = \left[\left(F_{yfl} - F_{yfr} \right)\sin\delta + \left(F_{xfr} - F_{xfl} \right)\cos\delta \right] l_s$$
$$+ \left(F_{xrr} - F_{xrl} \right) l_s - \left(F_{yrl} + F_{yrr} \right) l_r \qquad (3)$$
$$+ \left[\left(F_{xfr} + F_{xfl} \right)\sin\delta + \left(F_{yfr} + F_{yfl} \right)\cos\delta \right] l_f$$

Where the *xyz* coordinate system is the body-fixed coordinate system attached to the vehicle, in which x is the longitudinal axis of the vehicle, y is the lateral axis, and z is the vertical axis of the vehicle. V_x and V_y, represent the linear speed of the car in the x and y directions, respectively. The vehicle yaw rate is defined by r, and δ is the front wheels angle. Also, the mass and the moment of inertia of the car around the z axis are given by m and I_z, l_r and l_f denote the distance between the rear and front wheels from the center of gravity of the car. F_x and F_y represent the forces acting on the wheels in the wheel's body coordinate system.

According to Eqs. (1-3) for the dynamic modeling of the car, the forces acting on the wheels in both longitudinal and lateral directions must be calculated and determined. For this purpose, the Dugoff tire model [26, 27] has been used in this paper. Dugoff's model is used to calculate the forces generated by tires when both lateral and longitudinal forces are present. It assumes a uniform pressure distribution across the tire contact patch, simplifying the parabolic distribution used in the Pacejka model [28]. Despite this simplification, the model offers a key advantage by allowing independent tire stiffness values in both lateral and longitudinal directions. This is important because the stiffness of a tire can vary greatly between lateral and longitudinal forces. In comparison to the magic formula tire model, Dugoff's model is advantageous as it is derived analytically from force balance calculations. Additionally, the equations in Dugoff's model directly relate the lateral and longitudinal forces to the tire-road friction coefficient. Eqs. (4-5) show in detail how to calculate the longitudinal and lateral forces using the Dugoff tire model.

$$F_{xi} = C_l \frac{\lambda_i}{1+\lambda_i} f(D) \qquad (4)$$

$$F_{yi} = C_\alpha \frac{\tan(\alpha_i)}{1+\lambda_i} f(D) \qquad (5)$$

In this equation, λ_i represents the longitudinal slip coefficient, α_i is the slip angle, and C_l and C_α denote the longitudinal and lateral stiffness coefficients of the tire, respectively. Also, $f(D)$ is defined by:

$$f(D) = \begin{cases} (2-D)D & ; \quad D \leq 1 \\ 1 & ; \quad D \geq 1 \end{cases} \qquad (6)$$

$$D = \frac{\mu F_z (1+\lambda_i)}{2\left[\left(C_l \lambda_i \right)^2 + \left(C_\alpha \tan(\alpha_i) \right)^2 \right]^{\frac{1}{2}}} \qquad (7)$$

Where, F_z is the tire normal force, and μ is the coefficient of static friction between the tire and the road. The longitudinal slip coefficient for each wheel is defined by;

$$\lambda_i = \frac{R\omega_i - V_{xwi}}{\max(R\omega_i, V_{xwi})} \qquad (8)$$

Where, ω_i is the angular speed of each wheel and, V_{xwi} is the wheel speed in the longitudinal direction of the tire body coordinate according to Fig. 2.

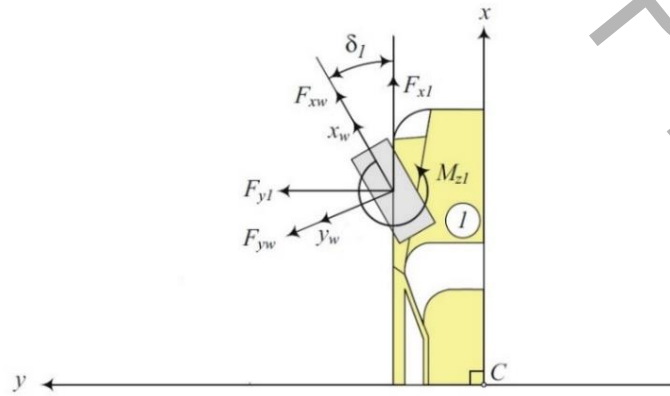By applying Newton's second law in Fig. 3, Eq. (9) is obtained.
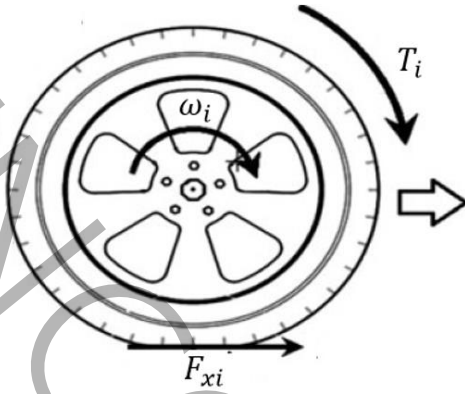

Fig. 2. Tire body coordinate system [29]

Fig. 3. Wheel Forces diagram [3]

$$J \dot{\omega}_i = T_i - R.F_{xi} \quad , i = fr, fl, rr, rl \quad (9)$$

Where, r is wheel radius, T_i is torque applied to the wheels F_{xi} and ω_i are denote frictional force and angular velocity of the wheel.

Due to the presence of independent electric motors in each wheel, the above equation can be directly applied in model. Eqs. (1-3), and Eq. (9) describe the 7-DOF model of the vehicle.

2- 2- Two layer controller

The Sliding Mode Control (SMC) method is recognized as one of the most robust control methods [30] . Its ease of operation and high robustness against uncertainties and noises make it a suitable choice for this paper. However, in practical scenarios, the phenomenon of chattering can be problematic in sliding mode control systems. This occurs due to delayed actuator operation and the inability to completely and perfectly follow control signals. To address the chattering issue, higher-order sliding mode control methods have been introduced. Higher-order sliding mode controllers allow the control system to zero not only the sliding variable but also the higher-order derivative of the sliding surface up to one order below the sliding mode controller's order. For instance, in second-order controllers, the first derivative of the sliding surface tends to zero as well. These controllers result in smoother control signals as the high-frequency oscillating controller is in a higher order of system derivatives. One of the commonly used higher-order sliding mode methods is the Super Twisting Sliding Mode Controller (STSMC)[31].

In this paper, the STSMC algorithm is employed to design longitudinal and lateral controllers. Among these controllers, one is referred to as the upper layer or lateral controller, responsible for determining the control torque. The remaining four-wheel torque controllers are known as the lower layer

or longitudinal controllers, assigned to determining the rotational torque for each wheel. Collectively, this set is referred to as a two-layer controller. The effectiveness of each wheel in providing control torque is calculated using the Torque Vectoring (TV) algorithm.

The goal of the lateral controller is to converge the yaw rate error of the vehicle to zero. This error is equivalent to the difference between the actual yaw rate, r, and the desired one, and to determine the desired yaw rate, Eq. (10) is used.

$$r_d = \frac{V_x}{(l_f + l_r) + k_{us} V_x^2} \delta \quad (10)$$

In Eq. (10), k_{us} represents the stability index, which is calculated according to the geometric characteristics of the vehicle.[21]

In this controller, the sliding surface and its derivative are defined as Eqs. (11-14).

$$S_l = r - r_d \quad (11)$$

$$\dot{s}_l = \dot{r} - \dot{r}_d = \rho - h_a M_z \quad (12)$$

$$\rho = \frac{1}{I_z} \Big[\big[(F_{yfl} - F_{yfr}) \sin \delta + (F_{xfr} - F_{xfl}) \cos \delta \big] l_s \\ + (F_{xrr} - F_{xrl}) l_s - (F_{yrl} + F_{yrr}) l_r \\ + \big[(F_{xfr} + F_{xfl}) \sin \delta + (F_{yfr} + F_{yfl}) \sin \delta \big] l_f \Big] - \dot{r}_d \quad (13)$$

$$h_a = -\frac{1}{I_z} \quad (14)$$

According to the STSMC algorithm, the lateral controller is defined by Eq. (15).

$$M_z = -I_z \left(\eta. |S|^{\frac{1}{2}} sign(S) + U_a + \rho_n \right) \\ \dot{U}_a = w sign(S) \quad (15)$$

Where ρ_n and ρ_d are respectively the nominal value and the value caused by the uncertainty of the parameter ρ , it means that $\rho = \rho_n + \rho_d$. So the non-deterministic parameters in the equations can be introduced as a two-part parameter including the nominal value and the tolerance value due to uncertainty in the form of Eq. (16).
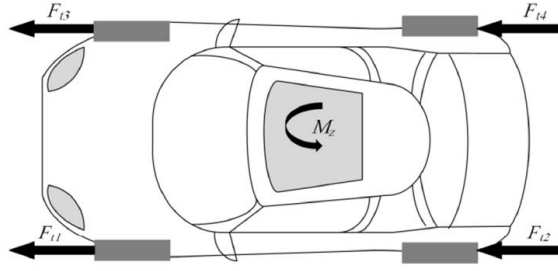
Fig. 4. Longitudinal forces acting on the wheels[10]

$$\mu = \mu_n + \mu_d$$
$$m = m_n + m_d$$
$$I_z = I_{zn} + I_{zd}$$
(16)

Considering that the torque M_z cannot be directly applied to the vehicle, the share of each wheel in providing this torque is calculated using the TV process [32]. According to the Fig. 4

$$M_z = \left[\left(F_{xfl} + F_{xrl} \right) - \left(F_{xfr} + F_{xrr} \right) \right] l_s$$
(17)

Therefore, the longitudinal forces of the wheels are adjusted in such a way as to provide M_z. This is done with different distribution strategies. In this paper, considering the limited capacity of each tire in bearing extra forces, it is assumed that each wheel will apply an equal share in providing the control torque M_z, which can be calculated according to the following equations.

$$\Delta F_{xi} = \frac{M_z l_i}{4}$$
(18)

This equation presents the required increase/decrease in longitudinal force for right/left (front and rear) wheels. Considering the slip rate has a direct relationship with the longitudinal forces according to Eqs. (4,6-7), using the first-order Taylor series as an inverse algorithm, the corresponding slip rate can be calculated for the new adjusted longitudinal force. Now, by placing the slip rate obtained as the desired slip rate of each wheel, the longitudinal controller for each wheel is designed. To this end, the sliding surface is defined in the form of Eqs. (19-20).

$$s_i = \lambda_i - \lambda_{f,i} \qquad , i=\text{fr,fl,rr,rl}$$
(19)

$$\lambda_i = \frac{R \omega_i - V_{x,i}}{\max \left(|R \omega_i|, |V_{x,i}| \right)}$$
(20)

Where $V_{x,i}$ represents the velocity component in the longitudinal direction of the wheel coordinate frame.

Again, according to STSMC algorithm, the longitudinal controller is defined by the following equations.

If $|R \omega_i| \ge |V_{x,i}|$

$$T_i = -\frac{J}{P_i} \left(\eta_i |S_i|^{1/2} sign(S_i) + U_i + \varphi_i \right)$$
(21)

Where

$$\varphi_i = -\left(\frac{P_i R F_{x,i}}{J} + \frac{\dot{V}_{x,i} |\omega_i|}{R \omega_i^2} \right)$$
$$P_i = \frac{|\omega_i|}{\omega_i^2} - \frac{1}{|\omega_i| \omega_i R} \left(R \omega_i - V_{x,i} \right)$$
(22)

And if $|rr.\omega_i| \le |V_{x,i}|$

$$T_i = -\frac{J V_{x,i}^2}{rr |V_{x,i}|} \left(\eta_i |S_i|^{1/2} sign(S_i) + U_i + \varphi_i \right)$$
(23)

In Eq. (23) φ_i is defined as

$$\varphi_i = -\left(Q_i + \frac{R^2 F_{x,i} |V_{x,i}|}{J V_{x,i}^2} \right)$$
(24)

Where

$$Q_i = \frac{\dot{V}_{x,i} |V_{x,i}|}{V_{x,i}^2} + \frac{\dot{V}_{x,i} R \omega_i}{|V_{x,i}| V_{x,i}} - \frac{\dot{V}_{x,i}}{|V_{x,i}|} \qquad (25)$$

In both conditions $|R\omega_i| \geq |V_{x,i}|$ and $|rr.\omega_i| \leq |V_{x,i}|$, U_i is defined as

$$\dot{U}_i = w_i \, sign(S_i) \qquad (26)$$

The torque calculated in Eqs. (21, 23) is applied as input torque to each wheel by IWM motors and the performance of the two-layer control system is completed.

2- 3- Extended Kalman Filter (EKF)

The previously proposed two-layer algorithm, as discussed in the previous section, offers the capability of controlling vehicle stability by receiving and processing sensor data. However, achieving increased effectiveness and higher productivity in designing different controllers for cars relies on accurate knowledge of the dynamic behavior of the real vehicle including state variables and vehicle physical parameters, and the mutual effects between the wheels and the road. To achieve this, various sensors are installed on the vehicle to record longitudinal and lateral accelerations, yaw rates, rotational torque of each wheel, etc.

To minimize the effects of noise and uncertainties on the sensor data and estimate the true conditions of the car, different types of observers or filters are applied to the sensor data. By making modifications to the filter equations, these filters can also be utilized to estimate various system parameters, such as the friction coefficient between the wheel and the road. This estimation process can be conducted online.

Various methods have been proposed to design state estimators. However, when assuming that the system information is contaminated with noise, the design of an optimal estimator based on Kalman filters is considered to remove the noise effects. Algorithms have been proposed to adapt the Kalman filter algorithm for nonlinear systems, one of which is the Extended Kalman Filter (EKF) algorithm. The EKF algorithm allows for the filtering process to be performed with simplicity and the momentary linearization of the system.

2- 3- 1- State estimation using EKF [33]

Assume that the measurement of the parameters is done at time t_k and this information is used to update the random system state vector x_k at time t_k. The state space equations for the nonlinear system in discrete time are defined in the form of Eqs. (27, 28).

$$x_{k+1} = f(x_k, u_k) + w_k \qquad (27)$$

$$y_k = g(x_k, u_k) + v_k \qquad (28)$$

In this equation, $f(.,.):(R^{n_x \times 1}, R^{n_u \times 1}) \to R^{n_x \times 1}$ is a nonlinear state equation and $w_k \in R^{n_x \times 1}$ is process noise, also $g(.,.):(R^{n_x \times 1}, R^{n_u \times 1}) \to R^{n_y \times 1}$ denotes nonlinear measurement function and $v_k \in R^{n_y \times 1}$ is measurement noise. In this method, the nonlinear state space model is linearized using the first-order Taylor series in the form of Eqs. (29- 30) [34].

$$x_{k+1}^- = A_k x_k^+ + u_k + w_k \qquad ;$$
$$A_k = \frac{\partial f_k(x_k, u_k)}{\partial u^T}\bigg|_{x=\hat{x}_k^+} \qquad (29)$$

$$y_{k+1} \cong C_{k+1} x_{k+1} + \tilde{z}_{k+1} + v_{k+1} \qquad ;$$
$$C_{k+1} = \frac{\partial g_{k+1}(x_{k+1}, u_{k+1})}{\partial x^T}\bigg|_{x=\hat{x}_{k+1}^-} \qquad (30)$$

It should be noted that proof of equations has been avoided for the sake of brevity. References [33, 34] should be used to check the proofs. It can be proved that.

$$\hat{x}_{k+1}^+ = \hat{x}_{k+1}^- + \bar{K}_{k+1}\left[y_{k+1} - C_{k+1}\hat{x}_{k+1}^-\right] \qquad (31)$$

$$\bar{K}_k = P_k^- C_k^T \left[C_k P_k^- C_k^T + R_k\right]^{-1} \qquad (32)$$

For posterior and prior estimation of covariance, respectively;

$$P_k^+ = \left(I - \bar{K}_k C_k\right) P_k^- \qquad (33)$$

$$P_k^- = A_{k-1} P_{k-1}^+ A_{k-1}^T + Q_{k-1} \qquad (34)$$

And by repeating the above algorithm at any moment, the estimation of the system state at that moment will be available.

2- 3- 2- State-parameter estimation using EKF

In addition to estimating the state of the system, the presented Kalman filter algorithms are also able to estimate the unknown parameters of the system. For this purpose, the augmented state vector is rewritten in the form of Eq. (35).

$$x' = \begin{bmatrix} x \\ p \end{bmatrix} \qquad (35)$$

Table 1. Physical parameters of the model

Parameter	Parameter Name	Value-Unit
m	The total mass of vehicle	1350 kg
I_z	Moment of inertia of vehicle	950 kg/m^2
l_s	Lateral distance between center of wheel from CG	0.75 m
l_r	Distance between rear wheels from CG	1 m
l_f	Distance between front wheels from CG	1.5 m
C_l	Longitudinal stiffness coefficient of the tire	30000
C_α	Lateral stiffness coefficient of the tire	40000
R	Wheel radius	0.32 m
J	Tire moment of inertia	1.07 kg/m^2

In this regard, the vector x is the state vector of the system and the vector **p** is the vector of the unknown parameters to be estimated. By placing x' instead of x in the EKF algorithm, a very good estimate of the unknown parameters **p** can be obtained using the measured data. This process is performed simultaneously with the estimation of the state of the system, x, and at the end, the estimation of the state and the unknown parameters of the system will be available at the same time [35].

According to Eq. (27), each of the states has an $f(x, u)$ relationship with other states and system inputs, and therefore such equations must be defined for the unknown parameters of p. In this article, wheel and road friction coefficients are estimated using the following model.

$$\mu_i = e^{-z_i} \tag{36}$$

Where z_i is a random first-order process with time constant τ which is defined as Eq. (37).

$$\tau_i \dot{z}_i + z_i = 0 \tag{37}$$

Therefore, the measurement, input, and state vectors are defined as follows.

$$y = \begin{bmatrix} a_x & a_y & r & \omega_{fr} & \omega_{fl} & \omega_{rr} & \omega_{rl} \end{bmatrix}^T \tag{38}$$

$$u = \begin{bmatrix} \delta & T_{fr} & T_{fl} & T_{rr} & T_{rl} \end{bmatrix}^T \tag{39}$$

$$x = \begin{bmatrix} V_x & V_y & r & \omega_{fr} & \omega_{fl} & \omega_{rr} & \omega_{rl} & z_{fr} & z_{fl} & z_{rr} & z_{rl} \end{bmatrix}^T \tag{40}$$

3- Simulations and Results

Simulations are conducted using the Matlab/Simulink software to validate the effectiveness of the proposed control strategy. A 7DOF vehicle model is utilized for the simulation, and the equations describing the model are given by Eqs. (1-9). The model parameters used in the simulation are presented in Table 1. The parameters of this table are defined and determined with a slight changes compared to the reference [36] . Uncertainty has been used in the definition of these parameters so that parameters such as mass and moment of inertia, which are subject to change due to the change in the number of passengers, are defined by combining a nominal value and an uncertain value in order to the simulation is more realistic, as mentioned in Eq. (16). The model and method
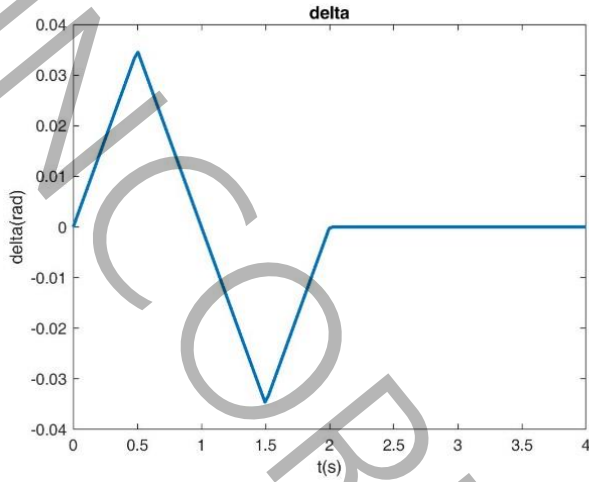
a. input steering angle
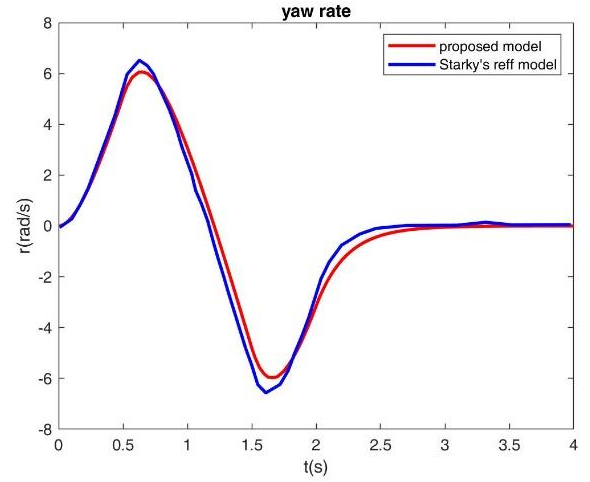
b. yaw rate
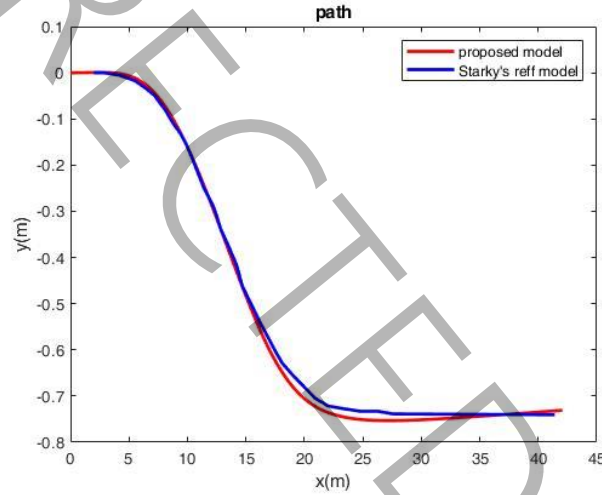
c. path

**Fig. 5. Model validation results compared to Smith and Starkey [25]**

used can be applied to different vehicles with different parameters, provided that it is four-wheeled and the power transmission system is similar to the definitions of this paper.

In the simulation process, the output vector of a 7-DOF vehicle model given by Eq. (38) as sensor outputs with nominal vehicle parameters including total mass are used for state estimation using EKF. In this algorithm, the friction coefficients are estimated by EKF using augmented states. The simulation is successful when the estimated friction coefficients are equal to the friction coefficients used in the real model and the vehicle tracks the desired yaw rate and path.

3- 1- Model validation

In order to verify the validity of the presented 7-DOF model, first, the dynamic response of the system to steering angle input is compared with one of the benchmark references [25]. Vehicle parameters and input steering angle are selected according to this reference. Fig. 5 shows the comparative results for the yaw rate (5b), and the vehicle path (5c). Fig. 5a shows the applied steering angle. It can be seen that the results are in full agreement with the reference model.
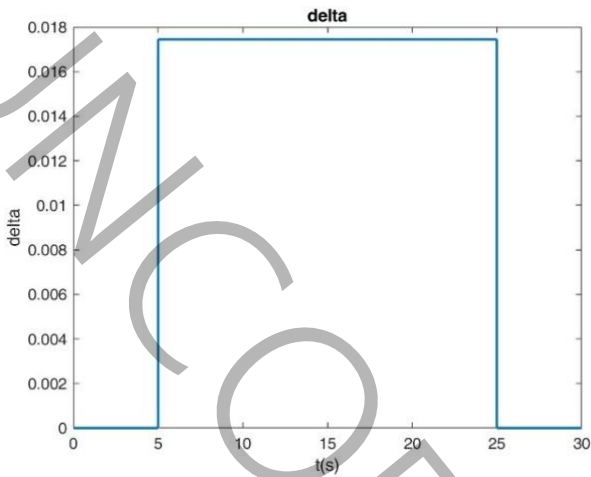
a. applied delta
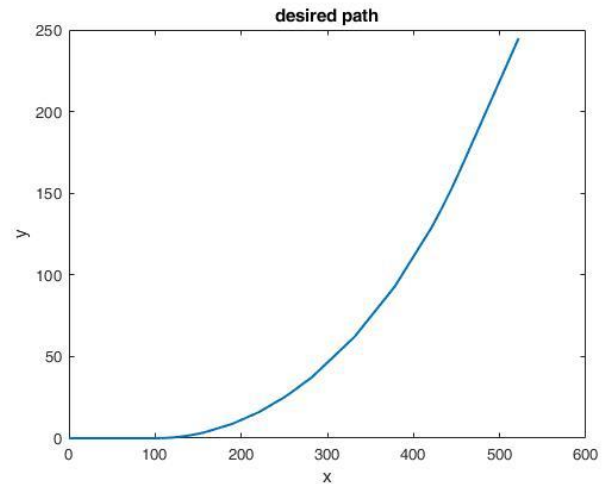
b. desired path

Fig. 6. Desired maneuver applied on vehicle

3- 2- Model and lateral controller

Now, we consider that only one lateral sliding mode controller is used, whose outputs, control torque, is directly applied to the system virtually.

By defining all system inputs, the desired maneuver is defined. Here it is assumed that $T_{fr} = T_{fl} = 60$ N.m, $T_{rr} = T_{rl} = 0$ N.m and $\mu=0.3$. Also, δ is defined in the form of Fig. 6a. The initial longitudinal speed of the system is $V_{x0} = 20$ m/s and finally the desired movement path of the system is drawn as Fig. 6b.

By implementing this algorithm, the response of the system to the maneuver defined above by applying the lateral controller is shown in Fig. 7. In this figure, comparisons have been conducted between open loop and close loop system parameters with desired values. Only the lateral controller is considered to be active. In Fig. 7a, the longitudinal velocity of the car is depicted. It is evident that the lateral controller has effectively maintained the longitudinal speed within a specific range. Fig. 7b illustrates the lateral speed of the car, which is significantly lower in the controlled mode. In Fig. 7c, the desired, controlled, and uncontrolled values of yaw rate are showcased. As anticipated, the controlled value closely aligns with the desired value, demonstrating the capability of the sliding mode control system to track the desired trajectory. Finally, Fig.7d presents the diagram of the desired, controlled, and uncontrolled states of the car's movement path. As expected, the system equipped with the controller successfully navigates in the desired direction, whereas the system without the controller deviates from the intended path.

3- 3- Torque vectoring process and longitudinal controllers

As mentioned, it is practically impossible to directly apply the calculated M_z in the lateral controller to the vehicle. Therefore, by using the TV process, the forces that be applied to each wheel is calculated and the torque applied to each engine is computed by the longitudinal controller and the system is controlled. In part 2, this process is fully described. The algorithm used in the previous section completed and the algorithm of Fig. 8 is obtained.

Fig. 9 illustrates the outcomes of the algorithm in Fig. 8 compared to the results obtained in the earlier section, which M_z was directly and unrealistically applied to the system.

Fig. 9a is the longitudinal speed diagram of the vehicle, which can be seen that by applying the T_i, its range of changes is less than before. Fig. 9b also shows the lateral speed changes. In Fig. 9c, the yaw rate changes are shown and it can be seen that by applying T_i, the convergence to the desired value is done much more accurately. Finally, Fig. 9d shows the path of the car in desired conditions, with the longitudinal controller, and without the longitudinal controller. It can be seen that the convergence to the desired path is improved by adding the longitudinal controller. In order to be able to make a numerical comparison of the proximity of the movement path to the desired path in two cases, with only lateral controller (case 1) and with lateral and longitudinal controller (case 2), the root mean square (RMS) coefficient of the tracking error is calculated for both cases. The results are shown in Table 2. As can be seen, the RMS coefficient is smaller for case 2, which indicates that it is closer to the desired path. That is, after the application
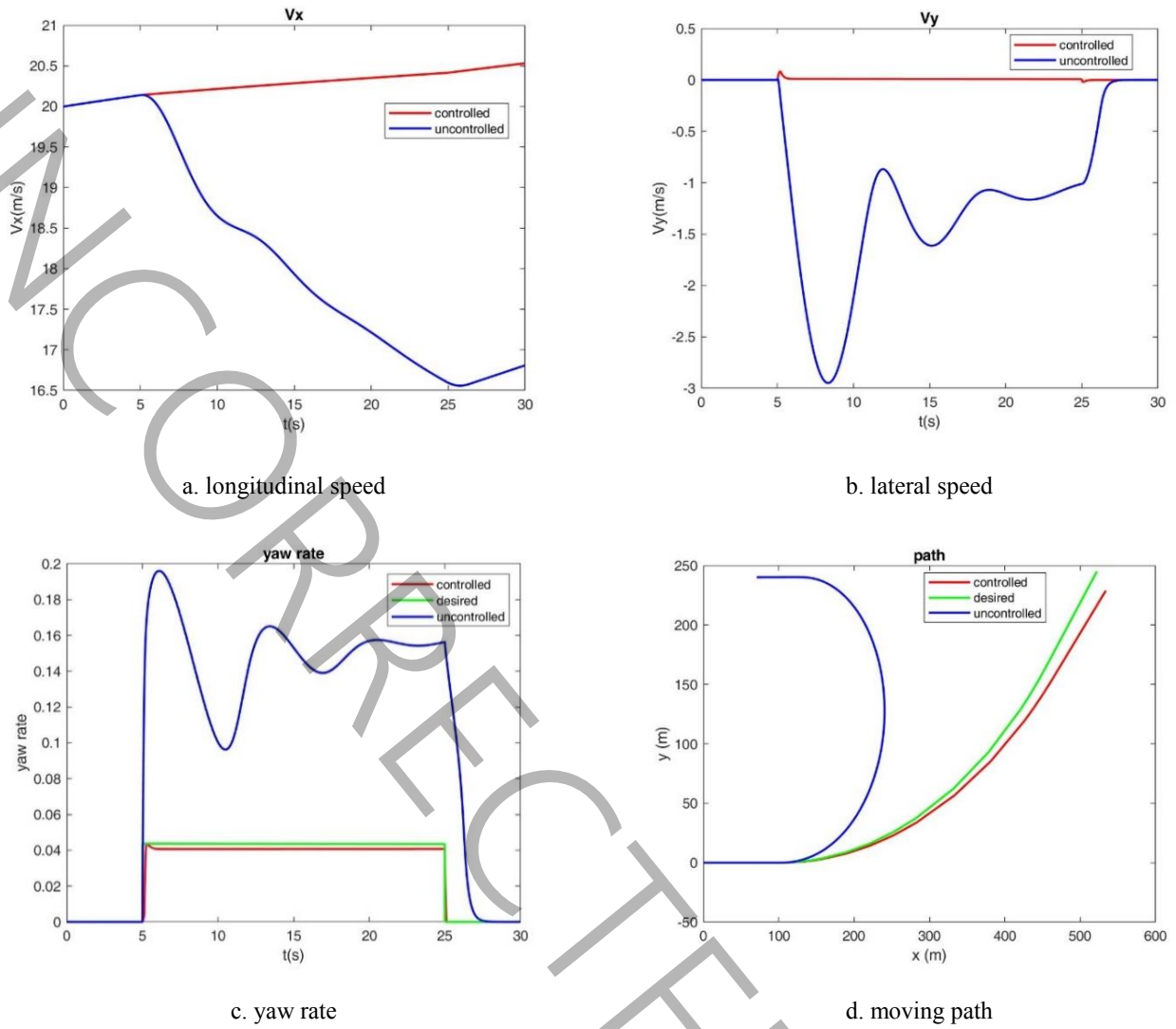
a. longitudinal speed

b. lateral speed

c. yaw rate

d. moving path

Fig. 7. Comparison of longitudinal and lateral speed and yaw rate and system movement path in modes with lateral controller and without controller
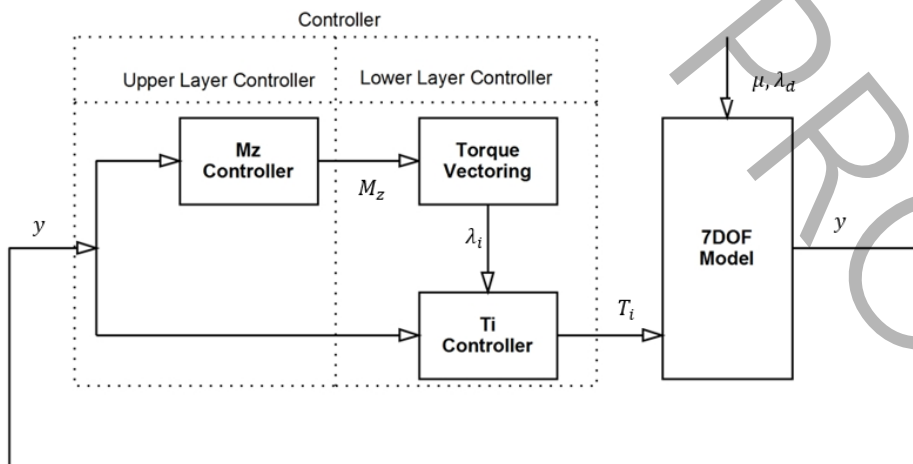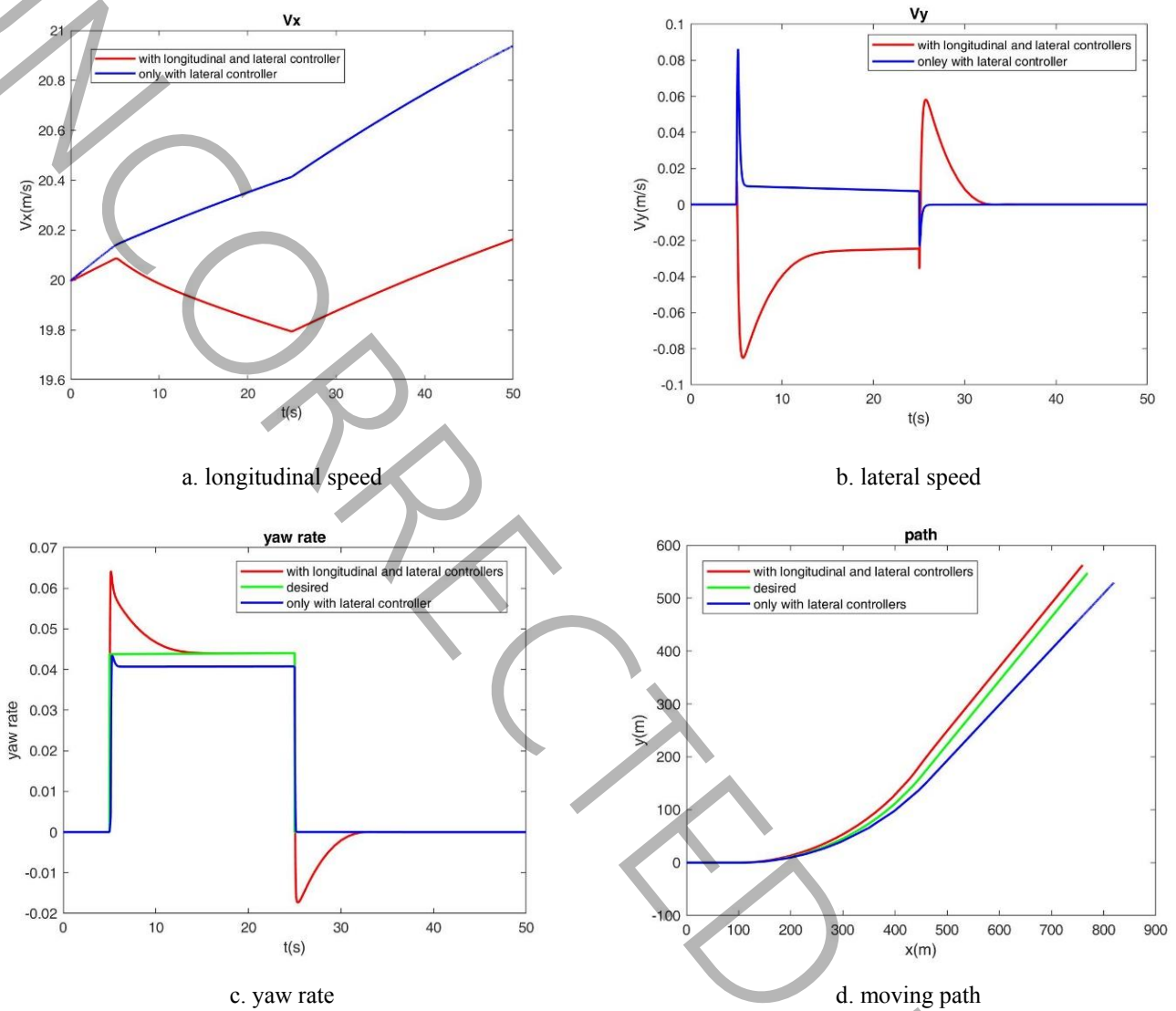

Fig. 8. Modified algorithm with TV and longitudinal controllers

a. longitudinal speed

b. lateral speed

c. yaw rate

d. moving path

Fig. 9. Comparison of longitudinal and lateral speed and yaw rate and system movement path in modes with only lateral controller and with longitudinal and lateral controllers

of longitudinal controllers, not only the system has become more realistic and the virtual actions become real actions, but the convergence of the system has also increased to the desired value, as can be seen.

To check how to apply T_i on the system, in Fig. 10, a comparative diagram of the changes in the rotation speed of the wheels for all four wheels is shown. It can be seen that at the moment of applying δ, two of the wheels register a positive change and the other two wheels register a negative change, and by applying these values, which are caused by applying the T_i, the is created in real and not virtual form.

3- 4- State and parameter estimation with joint-EKF

As mentioned in section 2.3, the use of controllers can be really useful when noise and uncertainties can be minimized from the data obtained from the sensors. Also, some unknown parameters, including the friction coefficient between the tire and the road, should be estimated online. In this article, joint-EKF is used to estimate the state and friction coefficient (each wheel separately) at the same time. Therefore, Fig. 11 shows the final algorithm is used.

Unlike the previous step, where the friction coefficients were assumed to be definite and equal to a constant number,

a. ω_{fr} b. ω_{fl}

c. ω_{rr} d. ω_{rl}
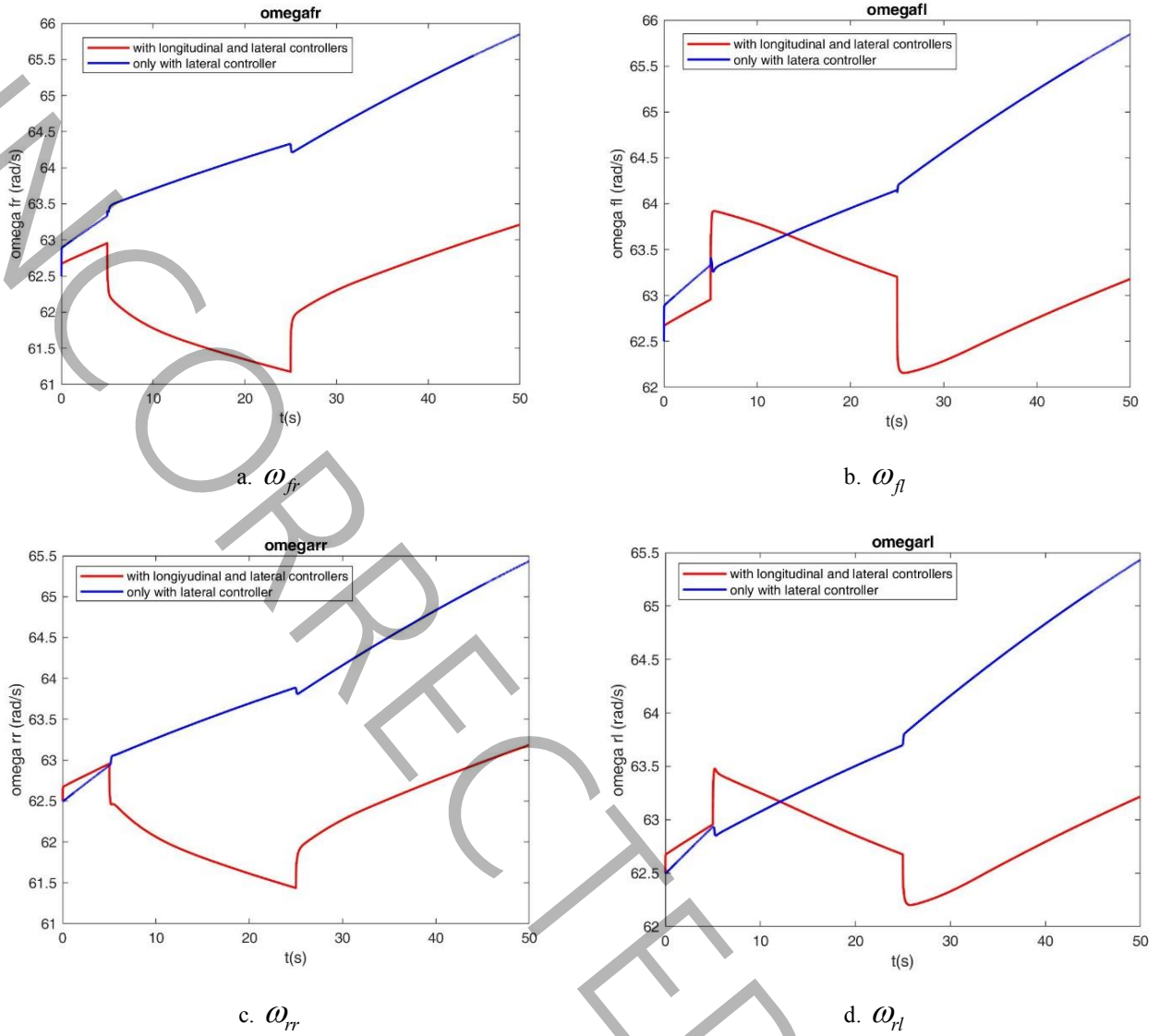
Fig. 10. Comparison of rotational speed of all four wheels in modes with only lateral controller and with longitudinal and lateral controllers
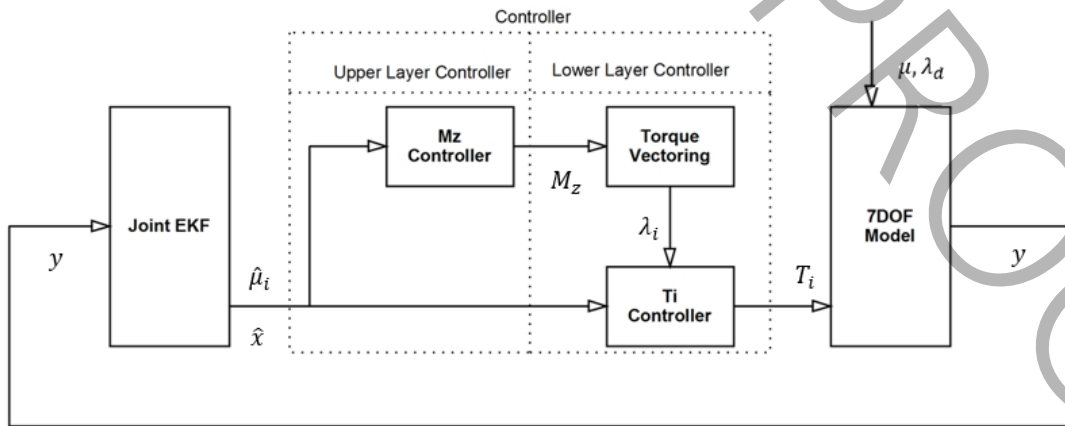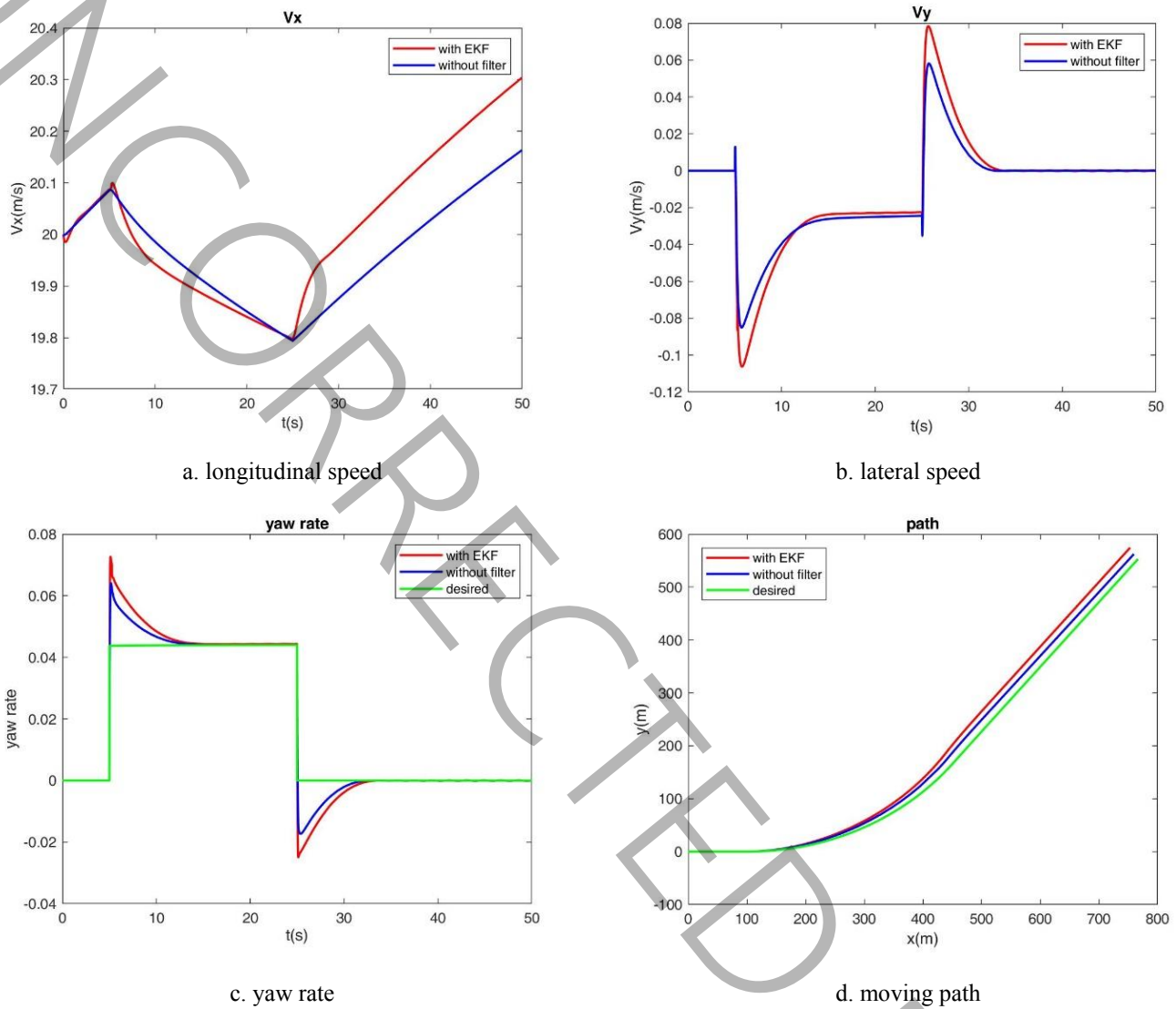

**Fig. 11. Modified algorithm with joint-EKF**

a. longitudinal speed

b. lateral speed

c. yaw rate

d. moving path

Fig. 12. Comparison of longitudinal and lateral speed and yaw rate and system movement path in modes with EKF and without it

in this step, these parameters are assumed to have uncertainty and are estimated. Therefore, in this step, the uncertainty has been calculated. Fig. 12 shows the parameters of the longitudinal and lateral velocities, the yaw rate and the movement path of the system in the states with Kalman filter and without it. It is clear that state graphs without filters are more appropriate answers, but we must not forget that by adding a filter, the system becomes one step more practical and can be used in more real examples. In other words, in order to make the used algorithm more practical, a cost is paid, which is a small distance from the ideal answer. RMS

coefficient of the tracking error is calculated in two cases, without filter (case 3) and with EKF (case 4). The results are shown in Table 2. As can be seen, the RMS coefficient is smaller for case 3, which indicates that it is closer to the desired path.

Fig. 13 shows the estimated and desired friction coefficients of the wheels separately for each wheel. It can be seen that the convergence process starts from the moment of applying the steering angle. It is carefully observed in the equations of the system that if the steering angle is zero, the change in the friction coefficient does not create a noticeable
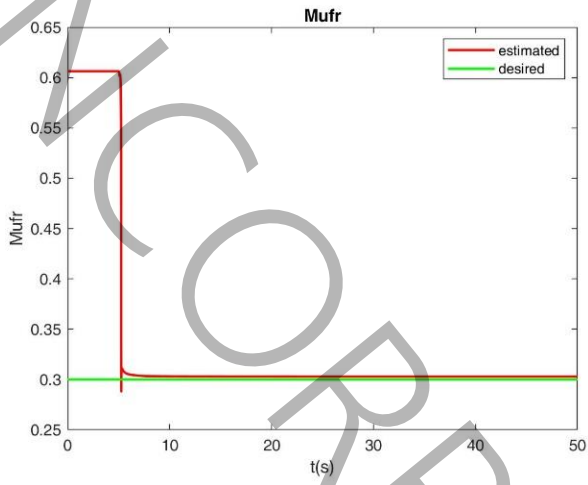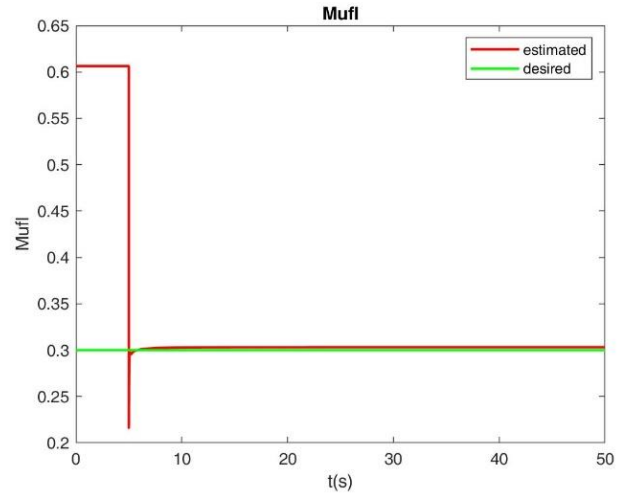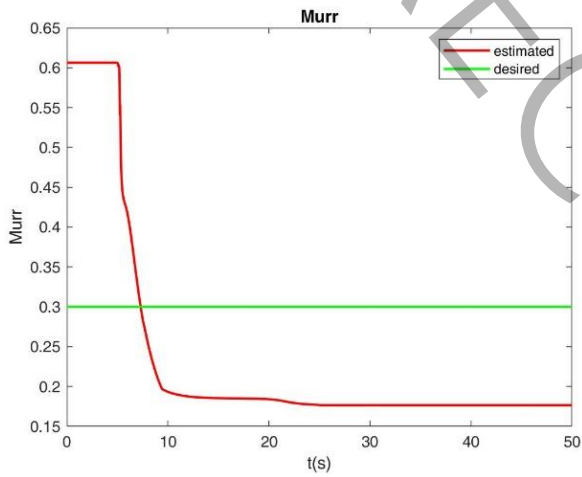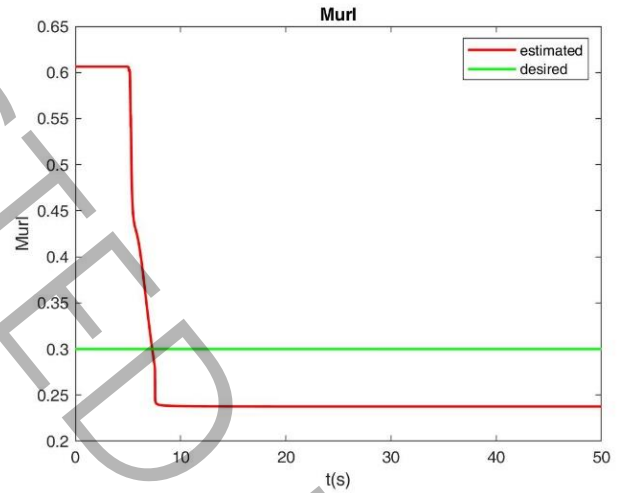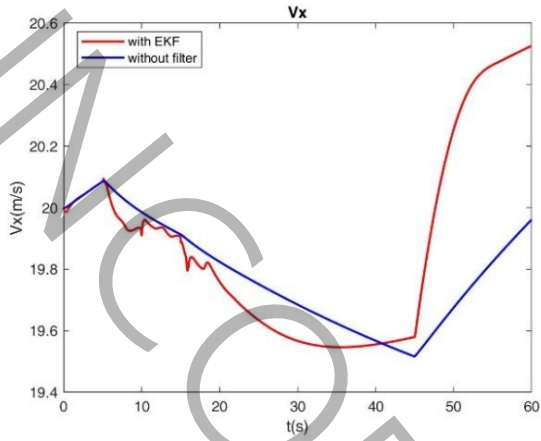
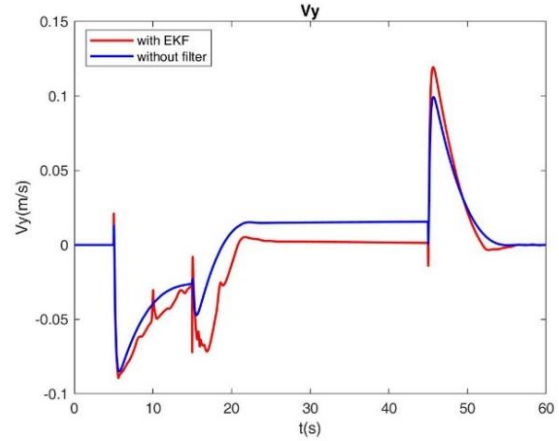**Fig. 13. The process of estimating the friction coefficient of wheels with EKF**

change in the parameters of the system state, and therefore these parameters are inestimable by filter in this state. It can also be seen that the estimation process is more accurate in the front wheels, this is because the steering angle is applied to the front wheels and the change in the friction coefficients of the front wheels causes a greater change in the parameters of the system state. And therefore, the filter is more sensitive in their estimation.

In the second case, a situation is considered where the friction coefficient between the tire and the road changes,

and the filter must estimate these coefficients for the second time. As it was said, the parameter estimation process is performed correctly when the steering angle is non-zero, so in this example, the time period of applying the steering angle increases from 5- 25 seconds to 5- 45 seconds. The desired friction coefficient from 0- 15 seconds is equal to 0.3 and then 0.6. Fig. 14 shows the state parameters of longitudinal and lateral velocities, yaw rate and movement path of the vehicle, as well as the estimated friction coefficients. It can be seen that the process of estimating the friction coefficients of the front
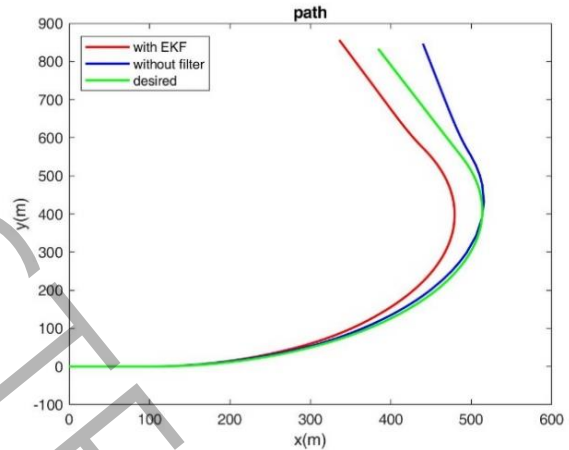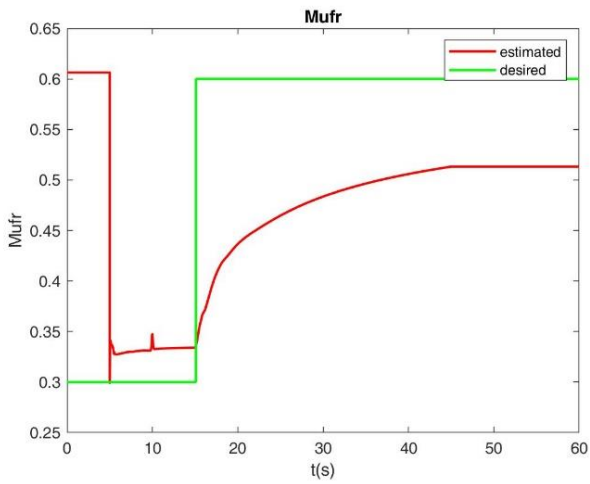
46

a. longitudinal speed
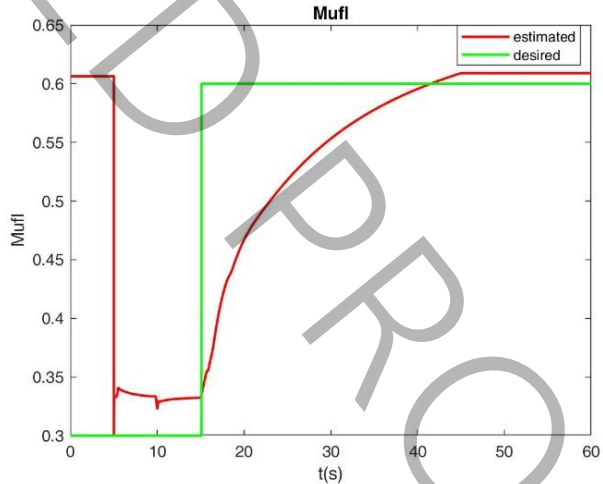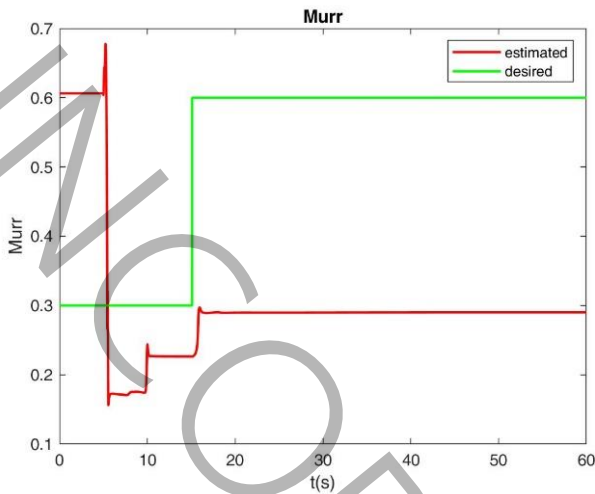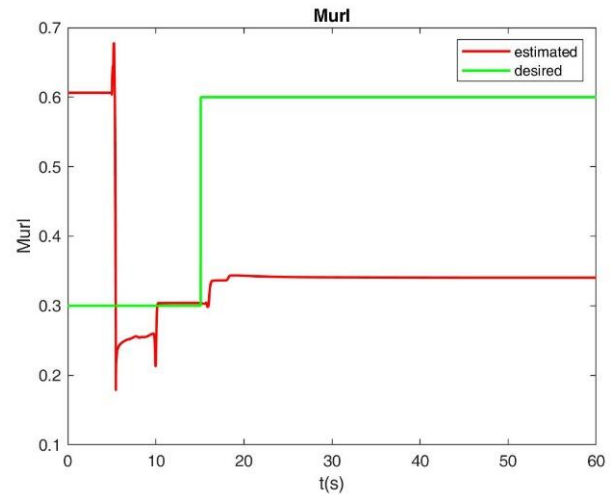

b. lateral speed

c. yaw rate

d. path

e. μ_{fr}
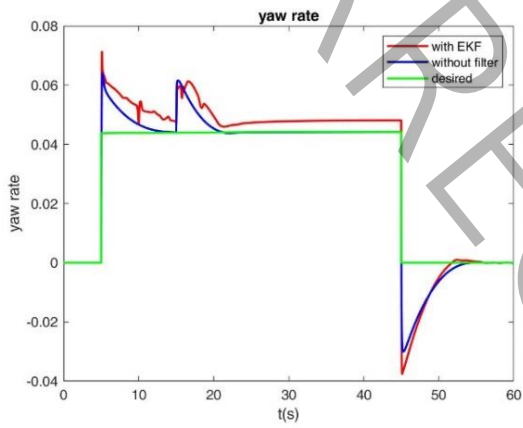
f. μ_{fl}

Fig. 14. The process of estimating the friction coefficient of wheels with EKF where the desired friction coefficient was changed(Continued)

Fig. 14. The process of estimating the friction coefficient of wheels with EKF where the desired friction coefficient was changed

Table 2. RMS coefficient of different modes

| Case name	Corresponding figure	RMS
case1		0.3682
	9d	
case 2		0.1907
case 3		0.1552
	12d	
case 4		0.2775
case 5		0.2403
	14d	
case 6		0.4750

wheels is acceptable. By checking the system's compliance with the desired yaw rate and the desired movement path, it can be seen that the estimation is generally effective. RMS coefficient of the tracking error is calculated in two cases, without filter (case 5) and with EKF (case 6). The results are shown in Table 2.

It should be noted that despite the difference between the estimated and desired friction coefficients, the system has been successful in controlling the vehicle. This is because some parameters such as m and also contain uncertainty, but since they are not estimated in the used algorithm, the burden of correcting the effect of these uncertainties is also applied to the estimated friction coefficients, and the system by changing the friction coefficients can also compensate the uncertainty of other parameters.
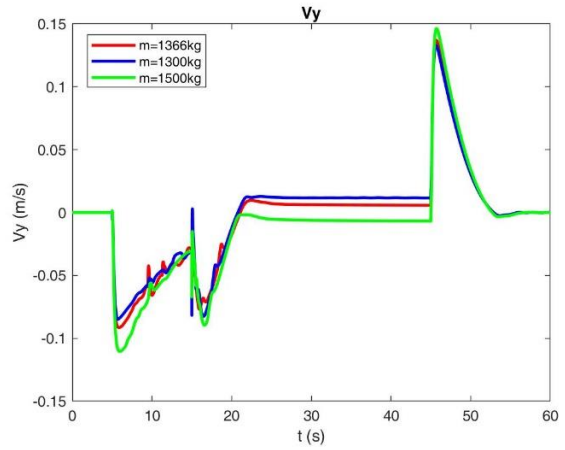
3- 5- Vehicle with different loads

In this section, the second example from the previous section is simulated for different vehicle loads. As mentioned earlier, the nominal weight of the vehicle is considered to be 1366 kg. To examine the effects of vehicle mass variation, which may result from changes in fuel levels or the number of passengers, the problem is also analyzed for masses of 1300 kg and 1500 kg. Fig. 15 illustrates the simulation results for different vehicle masses. Figs. a-d pertain to the vehicle's dynamic states, while Figs. e-h corresponds to the estimated friction coefficients. Other conditions remain the same as in the previous section, with filters and controllers activated. The results of Fig. 15 demonstrate the robustness of the algorithm against uncertainties in the system. This simulation was conducted using mass variations, which are among the
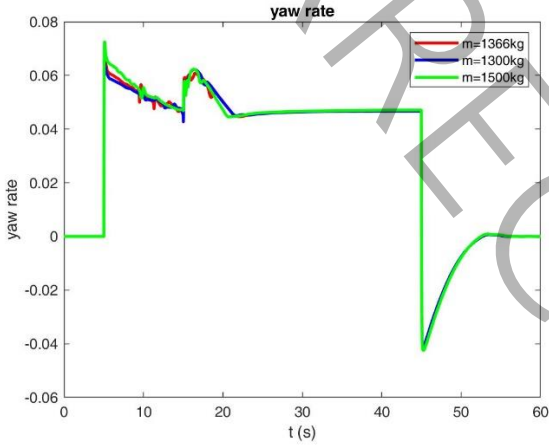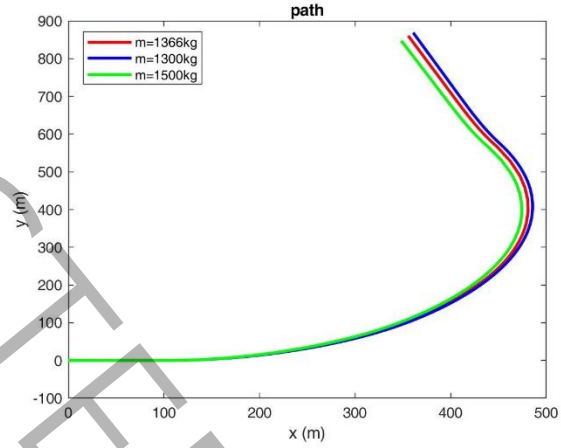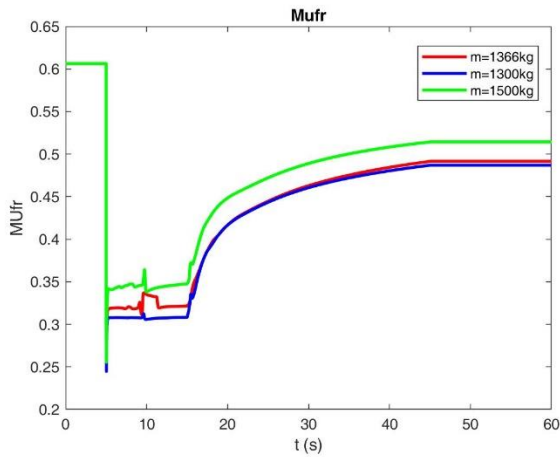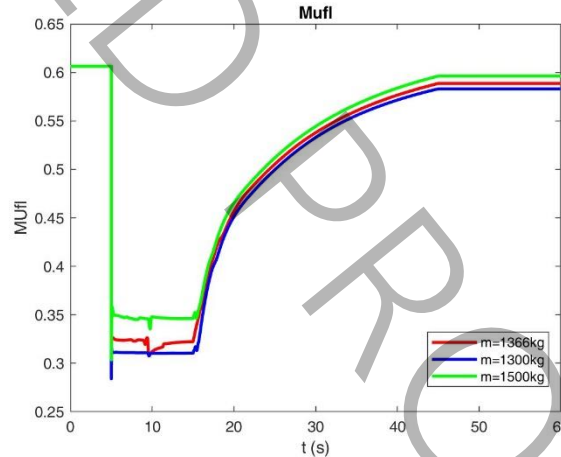
a. longitudinal speed

b. lateral speed

c. yaw rate

d. path

e. μ_{fr}
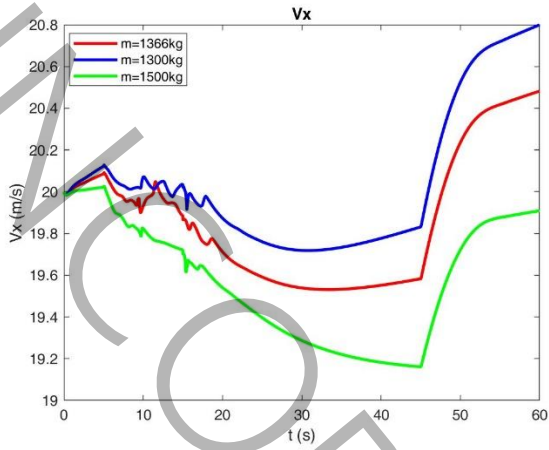
f. μ_{fl}

Fig. 15. Simulation results for vehicles with different loads. (Continued)
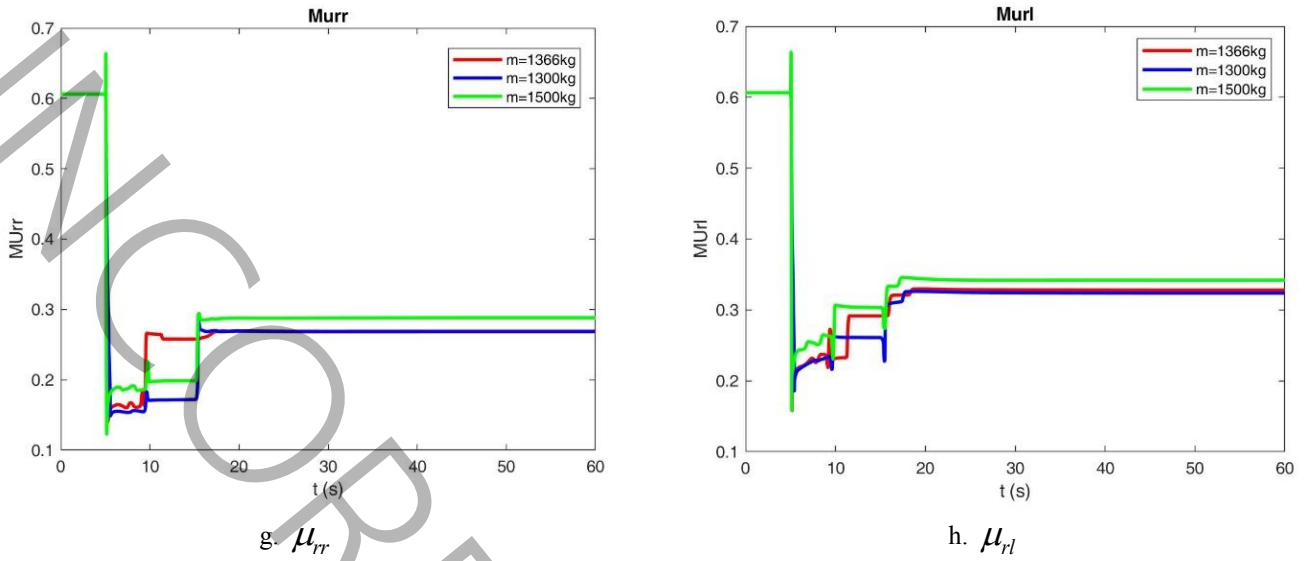
g. μ_{rr} h. μ_{rl}

Fig. 15. Simulation results for vehicles with different loads.

most significant factors contributing to vehicle dynamics uncertainty. The use of a Kalman filter, capable of reducing the effects of noise and uncertainties, combined with the application of sliding mode control, a highly robust control method, has resulted in an integrated robust algorithm.

4- Conclusion

A two-layer stability control method based on output feedback is employed for electric vehicle control with four in-wheel motors. The controller structure is based on Super-twisting sliding mode control and extended Kalman filtering (EKF). Joint-EKF simultaneously estimates vehicle state and TRFCs online. The upper layer controller calculates the control torque for lateral stability, while the lower layer controller determines individual wheel traction forces through torque vectoring. This approach ensures the upper layer's control torque is effectively implemented, maintaining vehicle stability and performance. The simulations show the vehicle command following in tracking the desired path by applying the control torque which is calculated in the upper layer controller. By using the TV algorithm and applying the control torques, calculated in the lower layer controller for each wheel separately, to the wheels, the vehicle tracks the desired path successfully. The EKF filter reduces the effects of noise and uncertainty on the measured data and at the same time estimates the vehicle state vector and TRFCs correctly. The results show that the presented algorithm has some errors in estimating friction coefficients in complex paths and conditions, although it was successful in following the desired path to a large extent.

5- Nomenclature

a_x	vehicle longitudinal acceleration, m/s²
a_y	vehicle lateral acceleration, m/s²
C_l	tire longitudinal stiffness, N/unit slip
C_α	tire lateral stiffness, N/rad
$F_{x,i}$	i-th tire longitudinal force, N
$F_{y,i}$	i-th tire lateral force, N
$F_{z,i}$	i-th tire vertical force, N
I_z	moment of inertia about z axis, kg/m²
l_f	distance of the CG to the front axle, m
l_r	distance of the CG to the rear axle, m
l_s	lateral distance between the center of the wheel from CG, m
J	tire inertia, kg/m²
$\bar{K}$	Kalman matrix
k_{us}	stability index
M_z	external yaw moment, N.m
m	vehicle total mass, kg
P	covariance matrix
R	tire radius, m
r	vehicle yaw rate, rad/s
s	sliding surface
T	vehicle applied torque, N.m
V_x	vehicle longitudinal velocity, m/s
V_y	vehicle lateral velocity, m/s
x	state vector of the system
y	output vector of the system

Greek symbols

δ	front tire steering angle, rad
λ	longitudinal tire slip

μ tire–road friction coefficient
ω tire angular velocity, rad/s

Subscript

d desired
fl front left
fr front right
rl rear left
rr rear right[1]

References

[1] S. He, X. Fan, Q. Wang, X. Chen, S. Zhu, Review on torque distribution scheme of four-wheel in-wheel motor electric vehicle, Machines, 10(8) (2022) 619.

[2] H. Zhang, C. Zhou, C. Wang, W. Zhao, An energy efficient control strategy for electric vehicle driven by in-wheel-motors based on discrete adaptive sliding mode control, Chinese Journal of Mechanical Engineering, 36(1) (2023) 58.

[3] T. Chen, L. Chen, X. Xu, Y. Cai, X. Sun, Simultaneous path following and lateral stability control of 4WD-4WS autonomous electric vehicles with actuator saturation, Advances in Engineering Software, 128 (2019) 46-54.

[4] B. Li, H. Du, W. Li, Y. Zhang, Side-slip angle estimation based lateral dynamics control for omni-directional vehicles with optimal steering angle and traction/brake torque distribution, Mechatronics, 30 (2015) 348-362.

[5] W. Wang, T. Ma, C. Yang, Y. Zhang, Y. Li, T. Qie, A path following lateral control scheme for four-wheel independent drive autonomous vehicle using sliding mode prediction control, IEEE Transactions on Transportation Electrification, 8(3) (2022) 3192-3207.

[6] M. Elbanhawi, M. Simic, R. Jazar, Receding horizon lateral vehicle control for pure pursuit path tracking, Journal of Vibration and Control, 24(3) (2018) 619-642.

[7] R. Marino, S. Scalzi, M. Netto, Nested PID steering control for lane keeping in autonomous vehicles, Control Engineering Practice, 19(12) (2011) 1459-1467.

[8] J. Guo, Y. Luo, K. Li, An adaptive hierarchical trajectory following control approach of autonomous four-wheel independent drive electric vehicles, IEEE Transactions on Intelligent Transportation Systems, 19(8) (2017) 2482-2492.

[9] J. Guo, Y. Luo, K. Li, Y. Dai, Coordinated path-following and direct yaw-moment control of autonomous electric vehicles with sideslip angle estimation, Mechanical Systems and Signal Processing, 105 (2018) 183-199.

[10] K. Liu, J. Gong, S. Chen, Y. Zhang, H. Chen, Model predictive stabilization control of high-speed autonomous ground vehicles considering the effect of road topography, Applied Sciences, 8(5) (2018) 822.

[11] H. Nam, W. Choi, C. Ahn, Model predictive control for evasive steering of an autonomous vehicle, International journal of automotive technology, 20 (2019) 1033-1042.

[12] H. Wang, B. Liu, X. Ping, Q. An, Path tracking control for autonomous vehicles based on an improved MPC, IEEE access, 7 (2019) 161064-161073.

[13] F.L. Silva, L.C. Silva, J.J. Eckert, M.A. Lourenco, Robust fuzzy stability control optimization by multi-objective for modular vehicle, Mechanism and Machine Theory, 167 (2022) 104554.

[14] G. Liu, S. Wang, D. Zhang, Y. Shen, Z. Yao, Fault Tolerant Control Allocation Based on Adaptive Sliding Mode Control for Distributed-Driven Electric Vehicle, in: Proceedings of 2019 Chinese Intelligent Automation Conference, Springer, 2020, pp. 251-261.

[15] X. Ji, X. He, C. Lv, Y. Liu, J. Wu, A vehicle stability control strategy with adaptive neural network sliding mode theory based on system uncertainty approximation, Vehicle System Dynamics, 56(6) (2018) 923-946.

[16] X. Ji, X. He, C. Lv, Y. Liu, J. Wu, Adaptive-neural-network-based robust lateral motion control for autonomous vehicle at driving limits, Control Engineering Practice, 76 (2018) 41-53.

[17] J. Chen, Z. Shuai, H. Zhang, W. Zhao, Path following control of autonomous four-wheel-independent-drive electric vehicles via second-order sliding mode and nonlinear disturbance observer techniques, IEEE Transactions on Industrial Electronics, 68(3) (2020) 2460-2469.

[18] A. Najafi, M. Masih-Tehrani, Lateral safety enhancement in a full dynamic vehicle model based on series active variable-geometry suspension, Journal of Computational Applied Mechanics, 52(1) (2021) 154-167.

[19] A. Najafi, M. Masih-Tehrani, A. Emami, M. Esfahanian, A modern multidimensional fuzzy sliding mode controller for a series active variable geometry suspension, Journal of the Brazilian Society of Mechanical Sciences and Engineering, 44(9) (2022) 425.

[20] A. Tahouni, M. Mirzaei, B. Najjari, Novel constrained nonlinear control of vehicle dynamics using integrated active torque vectoring and electronic stability control, IEEE Transactions on Vehicular Technology, 68(10) (2019) 9564-9572.

[21] A.N. Asiabar, R. Kazemi, A direct yaw moment controller for a four in-wheel motor drive electric vehicle using adaptive sliding mode control, Proceedings of the institution of mechanical engineers, part K: journal of multi-body dynamics, 233(3) (2019) 549-567.

[22] Z. Qin, L. Chen, M. Hu, X. Chen, A lateral and longitudinal dynamics control framework of autonomous vehicles based on multi-parameter joint estimation, IEEE Transactions on Vehicular Technology, 71(6) (2022) 5837-5852.

[23] Y. Wang, C. Lv, Y. Yan, P. Peng, F. Wang, L. Xu, G. Yin, An integrated scheme for coefficient estimation of tire–road friction with mass parameter mismatch

under complex driving scenarios, IEEE Transactions on Industrial Electronics, 69(12) (2021) 13337-13347.

[24] H. Alipour, M. Sabahi, M.B.B. Sharifian, Lateral stabilization of a four wheel independent drive electric vehicle on slippery roads, Mechatronics, 30 (2015) 275-285.

[25] D.E. Smith, J.M. Starkey, Effects of model complexity on the performance of automated vehicle steering controllers: Model development, validation and comparison, Vehicle system dynamics, 24(2) (1995) 163-181.

[26] H. Dugoff, P.S. Fancher, L. Segel, Tire performance characteristics affecting vehicle response to steering and braking control inputs, Highway Safety Research Institute, 1969.

[27] R. Rajamani, Vehicle dynamics and control, Springer Science & Business Media, 2011.

[28] H.B. Pacejka, E. Bakker, The magic formula tyre model, Vehicle system dynamics, 21(S1) (1992) 1-18.

[29] R.N. Jazar, Advanced vehicle dynamics, Springer, 2019.

[30] H.K. Khalil, Control of nonlinear systems, Prentice Hall, New York, NY, 2002.

[31] Y. Shtessel, C. Edwards, L. Fridman, A. Levant, Sliding mode control and observation, Springer, 2014.

[32] B. Najjari, M. Mirzaei, A. Tahouni, Design of optimal torque vectoring control system with predictive approach for improvement of stability and energy consumption in electric vehicle, Journal of Mechanical Engineering, 49 (2020) 257-267.

[33] M.S. Grewal, A.P. Andrews, Kalman filtering: Theory and Practice with MATLAB, John Wiley & Sons, 2014.

[34] D. Simon, Optimal state estimation: Kalman, H infinity, and nonlinear approaches, John Wiley & Sons, 2006.

[35] H. Heidfeld, M. Schünemann, R. Kasper, UKF-based State and tire slip estimation for a 4WD electric vehicle, Vehicle System Dynamics, 58(10) (2020) 1479-1496.

[36] A. Ferrara, C. Vecchio, Low vibration vehicle traction control to solve fastest acceleration/deceleration problems via second order sliding modes, in: 2007 American Control Conference, IEEE, 2007, pp. 5236-5241.